Nigerian Journal of Applied Physics (NJAP)
ISSN Print: 3115-5871
ISSN Online: 3115-588X
DOI: https://doi.org/10.62292/njap-v2i3-2026-113
Volume 2(3), September 2026

Density Functional Theory Assessment of the Structural, Electronic and Optical Properties of Lead-Free $KSnI_3$ Perovskite

***[1]Samuel Adebayo, [2]Adetunji Bamidele Ibrahim, [1]Olusola Akinrinola, [1]Mojoyinola Kofoworola Awodele, and [1]Ayodeji Oladiran Awodugba**

[1]Department of Pure and Applied Physics, Ladoke Akintola University of Technology, Ogbomoso, Oyo State, Nigeria.
[2]Bells University of Technology, Ota, Ogun State, Nigeria.

*Corresponding author's email: samadeyemi29@gmail.com

ABSTRACT
Lead-free halide perovskites are of interest for optoelectronic applications, but the electronic and optical properties of potassium tin iodide ($KSnI_3$) require further assessment. Here, we performed density functional theory calculations using Quantum ESPRESSO 7.2 to examine its structural, electronic, and optical properties. The optimised structure yielded a characteristic lattice parameter of approximately 6.30 Å. The calculated band gap was approximately 0.75 eV, indicating semiconducting behaviour; this GGA-PBE result is method-dependent, and spin–orbit coupling was not included. The density of states indicates that iodine 5p states dominate the valence-band region, with tin 5s hybridisation, while tin 5p states contribute strongly to the conduction band. Optical calculations show a weak response below approximately 2.52 eV, followed by increased absorption and stronger dielectric and related optical features at higher photon energies. These results provide a theoretical description of $KSnI_3$ and motivate further study. The optimised structure and bulk DFT results alone do not establish thermodynamic stability or photovoltaic device performance; phase competition, lattice dynamics, spin-orbit effects, and experimental or device-level validation remain important avenues for future work.

Keywords:
$KSnI_3$,
Lead-Free Perovskite,
Density Functional Theory,
Density of States,
Optical Properties.

INTRODUCTION

Metal-halide perovskites are generally described by the ABX_3 framework, in which A is a monovalent cation, B is a divalent cation, and X is a halide anion. Their corner-sharing BX_6 octahedral networks provide a chemically versatile platform in which composition, lattice distortion, octahedral tilting, and strain can modify orbital overlap, band dispersion, carrier transport, and optical transitions (Aberle, 2009). These characteristics have made halide perovskites important candidates for photovoltaic and optoelectronic applications. Nevertheless, the widespread use of lead-based absorbers raises concerns about toxicity, environmental release, and end-of-life management. Replacing Pb^{2+} with a less toxic divalent cation is therefore an important materials-design objective, provided that the resulting compound retains suitable structural integrity and optoelectronic functionality. Tin is one of the most closely related substitutes because Sn^{2+} is isovalent with Pb^{2+} and can form analogous tin-halide frameworks. However, lead-free tin perovskites do not provide a simple one-for-one solution. Sn^{2+} is susceptible to oxidation to Sn^{4+}, and this chemical instability can generate defects, increase background carrier concentrations, accelerate recombination, and reduce device stability. Tin-halide materials may also exhibit phase competition, structural distortion, and sensitivity to oxygen, moisture, temperature, and processing conditions. Macdonald et al. (2023) therefore emphasised that progress in tin-based photovoltaics depends on integrated control of composition, additives, interfaces, and degradation pathways rather than band-gap optimisation alone. The motivation for studying $KSnI_3$ is consequently both environmental and fundamental: it offers a lead-free composition whose structural and electronic behaviour must be established before credible device-level claims can be made (Adebayo et al., 2026).
$KSnI_3$ combines an alkali-metal A site, a tin B site, and a highly polarizable iodide sublattice. In the ideal perovskite picture, K^+ occupies the larger cavity formed by the SnI_6 framework, while Sn^{2+} is coordinated by

iodide ions. The relatively small size of K^+ compared with the iodide framework can promote octahedral tilting and lower-symmetry distortions rather than guaranteeing an undistorted cubic structure. Accordingly, a cubic $KSnI_3$ model should be treated as a high-symmetry reference unless its energetic, dynamical, and structural stability has been demonstrated explicitly. Phase assignment is particularly important because crystal symmetry affects band-edge locations, direct or indirect band-gap character, orbital hybridisation, anisotropic optical response, and the interpretation of calculated lattice parameters. Prior first-principles work has examined orthorhombic $KSnI_3$ and reported structural, electronic, and optical properties for that phase, including a band gap within the stated computational framework (Pindolia et al., 2023). Other work has considered several $KSnI_3$ polymorphs and found that orthorhombic and monoclinic structures can exhibit different stability and band-gap characteristics, while some high-symmetry tetragonal models may be dynamically unstable (Ayvalik et al., 2026). Comparative calculations on $XSnI_3$ compositions have likewise shown that predicted gaps and optical responses vary with the A-site cation and the adopted theoretical treatment (Chatzisideris et al., 2016). These findings establish that $KSnI_3$ cannot be discussed rigorously without specifying its phase, space group, relaxed geometry, and calculation conditions.

The oxidation state of tin adds a further layer of complexity. The intended $KSnI_3$ composition contains Sn^{2+}, but oxidation toward Sn^{4+} can alter stoichiometry, defect chemistry, carrier density, and the stability of a prospective absorber (Chopra et al., 2004). A ground-state structural calculation alone cannot establish resistance to oxidation or operational device stability (Das et al., 2022). It can, however, provide a controlled basis for examining the relationship between the selected crystal structure, electronic states, and optical transitions. This distinction is essential when interpreting first-principles results as materials evidence rather than as direct proof of photovoltaic performance.

Despite the growing number of calculations on $KSnI_3$ and related tin-halide perovskites, the available evidence is not yet fully comparable across studies (Deepika et al., 2025). Reported band gaps and optical onsets may differ because authors use different phases, lattice parameters, exchange-correlation functionals, pseudopotentials, plane-wave cutoffs, Brillouin-zone meshes, spin-orbit-coupling treatments, and optical-response formalisms. In addition, a relaxed total-energy minimum is sometimes described as proof of thermodynamic stability even when formation energies against competing phases, elastic properties, phonon spectra, finite-temperature effects, or phase-energy comparisons have not been reported (Kheswa et al., 2025). These methodological differences make it difficult to determine whether apparent disagreements reflect genuine material behaviour or differences in computational protocol (Kundara and Baghel, 2025a).

A further limitation is the incomplete connection between structural, electronic, and optical results. A band plot or density-of-states curve is not sufficient by itself to establish whether the fundamental gap is direct or indirect; the valence-band maximum and conduction-band minimum must be identified in reciprocal space. Similarly, an optical absorption onset cannot be compared directly with an electronic band gap unless the functional, relativistic treatment, broadening, transition matrix elements, polarization, and plotting conventions are consistent (Kundara and Baghel, 2025b). The literature therefore supports the need for a phase-aware and reproducibility-oriented investigation, but it does not justify an absolute claim that $KSnI_3$ has never been studied. The contribution of the present work is consequently methodological and integrative rather than a claim of first discovery (Pindolia and Shinde, 2023a). It establishes a documented first-principles workflow for $KSnI_3$ that links structural and energetic optimization with orbital-resolved electronic analysis and optical-response calculations. Phase assignment, exchange–correlation dependence, and spin–orbit coupling are treated as interpretation variables to be disclosed in accordance with the calculations performed (Pindolia and Shinde, 2023b). By distinguishing previously published findings from the present calculations, and verified outputs from unresolved stability or device-performance questions, the work seeks to improve the reproducibility and evidential strength of $KSnI_3$ materials assessment (Pindolia and Shinde, 2023c). This framework is intended to provide a more reliable basis for comparison with other lead-free perovskites and to identify calculations needed before photovoltaic feasibility can be inferred.

In the present study, structural and energetic optimisation is combined with analysis of the band structure, total and orbital-projected densities of states, and frequency-dependent optical response. The optical quantities considered include the dielectric function, absorption coefficient, refractive index, extinction coefficient, reflectivity, energy-loss function, and transmittance (Sabino et al., 2024). The calculations are implemented in Quantum ESPRESSO 7.2, and their interpretation is conditioned on the adopted exchange-correlation functional, pseudopotential, Brillouin-zone sampling, convergence criteria, and relativistic treatment (Said and Elkhattabi, 2024). The work does not claim definitive thermodynamic stability, resistance to Sn^{2+} oxidation, or photovoltaic device efficiency in the absence of direct supporting calculations or experimental evidence.

Accordingly, this study aims to use a phase-aware density functional theory workflow implemented in Quantum ESPRESSO 7.2 to characterise the structural, energetic, electronic, and optical properties of the $KSnI_3$ crystal model, including its optimised geometry, band structure

and orbital contributions near the band edges, and frequency-dependent optical response.

The Governing Equations

The Nominal Composition of the Perovskite

$$KSnI^3 = ABX^3;\ \ A = K,\ B = Sn,\ X = I \quad (1)$$

$KSnI_3$ is represented by the chemical formula ABX_3, where the A site is occupied by a monovalent potassium cation (K^+), the B site by a divalent tin cation (Sn^{2+}), and the X sites by three iodide anions (I^-). Charge neutrality is maintained as $K^+ + Sn^{2+} + 3I^- = 0$, which also defines the stoichiometry, atomic count in the primitive cell, electron count, and nominal coordination topology. In the cubic perovskite structure, Sn is coordinated to six I atoms forming a SnI_6 octahedron, with K situated in the larger cavity formed by corner-sharing octahedra. It is crucial to note that the ABX_3 notation does not confirm the cubic phase as the ground state. Factors such as octahedral tilting, lower-symmetry distortions, temperature variations, strain, and competing phases can influence the stability of the crystal structure (Sharma et al., 2024).

Electronic Hamiltonian

$$\hat{H}_e = -\sum_i (\hbar^2/2m_e)\nabla_i^2 - \sum_i^I \sum_i (Z^I e^2/4\pi\varepsilon_0|r_i - R^I|) + \sum_i < _j e^2/(4\pi\varepsilon_0|r_i - r_j|) \quad (2)$$

The many-electron Hamiltonian under the Born-Oppenheimer approximation for fixed nuclei includes three main terms: the kinetic energy of electrons, the attractive Coulomb interaction between each electron and nucleus, and the repulsion between electrons (Sumona et al., 2023). The nuclear–nuclear repulsion, while constant in electronic coordinates, is essential for comparing total energies across different geometries. In practical applications like plane-wave DFT, the nuclear potential transitions to a pseudopotential approach, simplifying the treatment of the many-body wavefunction to focus on electron density (Sundaram et al., 2018).

Hohenberg-Kohn Energy Functional

$$E[n] = T_s[n] + E_{ext}[n] + E^H[n] + E_{xc}[n] + E^{II} \quad (3)$$

The Hohenberg–Kohn energy functional provides a framework for expressing total energy as a function of ground-state electron density n(r). It includes $T_s[n]$ (kinetic energy of a non-interacting system), $E_{ext}[n]$ (interaction with external nuclei), $E^H[n]$ (Hartree electrostatic energy), and $E_{xc}[n]$ (exchange–correlation functional addressing kinetic energy differences and non-classical effects). E^{II} represents ion–ion repulsion. Due to the unknown exact total-energy functional, practical calculations rely on approximations like local-density approximation or hybrid functionals, impacting the reliability of various material properties (Tarekuzzaman et al., 2025).

Electron Density from Kohn-Sham Orbitals

$$n(r) = \Sigma\sigma\, \Sigma k\, w_k\, \Sigma m\, f_{mk}\sigma\, |\psi_{mk}\sigma(r)|^2 \quad (4)$$

Where, n(r) is the electron density, σ is the spin index, k labels the Brillouin-zone point, w_k is its integration weight, m is the band index, $f_{mk}\sigma$ is the occupation, and $\psi_{mk}\sigma$ is the corresponding Kohn–Sham orbital (Verma et al., 2023).The electron density in Density Functional Theory (DFT) is derived from occupied Kohn–Sham orbitals $\psi_{nk}(r)$, where n represents the band index and k is the crystal wavevector. The occupation factor f_{nk} indicates the occupancy of a state, typically being 0 or 1 at zero temperature, with fractional occupations for states near the Fermi level using smearing methods (Vishnupriya and Sathya, 2025). In a periodic solid, the expression incorporates a Brillouin-zone sum and, if necessary, factors for spin degeneracy. The density n(r) is crucial for forming the effective potential, which allows for iterative solutions of the Kohn–Sham equations until self-consistency is achieved. The integral of n(r) over the unit cell gives the number of valence electrons in the system (Wang et al., 2020).

Kohn-Sham Equation

$$[-(\hbar^2/2m_e)\nabla^2 + V_{ext}(r) + V^H(r) + V_{xc}(r)]\,\psi_{nk}(r) = \varepsilon_{nk}\,\psi_{nk}(r) \quad (5)$$

The Kohn-Sham equation is an eigenvalue problem that aims to replicate the ground-state density of an interacting system through a self-consistent approach, using an exchange-correlation approximation. It comprises a kinetic operator and considers external, Hartree, and exchange-correlation potentials, collectively forming the effective Kohn-Sham potential (Wang et al., 2020). The eigenvalues obtained are vital for understanding band structures and density-of-states plots but may not accurately reflect electron addition or removal energies. This is particularly relevant for materials like $KSnI_3$, where factors like semilocal functionals and spin–orbit coupling significantly influence the estimated band gap (Wang et al., 2021). The equation is solved iteratively until convergence criteria for density or total energy are achieved.

Hartree Potential

$$V^H(r) = [e^2/(4\pi\varepsilon_0)] \int n(r')/|r - r'|\, dr' \quad (6)$$

The Hartree potential is the electrostatic potential stemming from electron density, with the integration variable r′ representing the source position relative to the observation position r. It emphasises nearby charge through the Coulomb kernel $1/|r-r'|$ (Wang et al., 2022). In infinite periodic crystals, a periodic electrostatic method is necessary to evaluate the integral, avoiding

divergence from naive isolated-space integrals. The Hartree term primarily accounts for electron–electron repulsion, excluding exchange, correlation, and self-interaction corrections, which are addressed through V_{xc}. In plane-wave codes, this potential is often computed efficiently in reciprocal space using the density's Fourier components.

Exchange-Correlation Potential

$$V_{xc}(r) = \delta E_{xc}[n]/\delta n(r) \quad (7)$$

The exchange–correlation potential is derived from the exchange-correlation energy relative to electron density, crucial for resolving the Kohn-Sham problem after choosing an approximation for $E_{xc}[n]$ (Wang et al., 2024). In local or semilocal functionals, V_{xc} is density-dependent and may involve gradient terms. Hybrid functionals include a partly nonlocal exchange aspect. Its derivative nature indicates V_{xc} is not a freely adjustable potential but must align with the related energy functional to ensure consistency, critical for accurate structural relaxation and energy analyses. For $KSnI_3$, the chosen functional impacts lattice constants, phase ordering, orbital hybridisation, and the band gap size.

Structure, Phase Selection, and Stability

The structure, phase selection, and stability of cubic $KSnI_3$, with a nominal space group of $Pm\bar{3}m$, feature potassium (K) at the A site, tin (Sn) at the body-centred B site, and iodine (I) at the face-centered anion positions. This configuration serves as a valuable reference due to its clarity in showcasing the connectivity of the SnI_6 framework and providing a compact primitive cell. However, it is not necessarily the ground state; a thorough investigation should include a variety of lower-symmetry tilt patterns, assessing their relaxed energies, force residuals, stress tensors, and where applicable, phonon spectra (Wang et al., 2024). While tolerance-factor estimates may assist in preliminary screening, they cannot replace comprehensive total-energy and dynamical-stability analyses.

Ayvalik et al. (2026) conducted a relevant study on $KSnI_3$ polymorphs, comparing stability and band-gap characteristics across orthorhombic, monoclinic, and tetragonal phases. Their findings indicate that the assertion "$KSnI_3$ has a band gap of 0.65eV" is insufficient without specifying the respective phase, relaxed geometry, functional, spin-orbit coupling treatment, and temperature consideration

MATERIALS AND METHODS

In this study, we conducted a first-principles investigation to analyze the structural, electronic, and optical properties of lead-free potassium tin iodide ($KSnI_3$) perovskite. The research aimed to provide a comprehensive understanding of the crystal structure, energetics, electronic states, and frequency-dependent optical response of $KSnI_3$. All calculations were performed at zero temperature. The structural, electronic, and lattice dynamics of $KSnI_3$ perovskite compositions were thoroughly studied using Density Functional Theory (DFT) and pseudopotential plane wave methods implemented in the Quantum Espresso 7.2 code. The investigation employed projected augmented-wave (PAW) pseudopotentials from pslibrary with the Perdew-Burke-Ernzerhof (PBE) functional to define the exchange-correlation interactions (Yadav and Sharma, 2024). Additionally, specific computational parameters were established, with a cutoff energy set at 80 Ry and a k-points mesh configured to 8 × 8 × 8 for both wave function calculations and Brillouin zone integrations. The chosen computational protocol was designed to achieve a balance between the precision necessary for analyzing a heavy-element halide perovskite and the numerical convergence required for consistent comparisons across various structural, electronic, and optical properties.

Computational Model and Phase Protocol

$KSnI_3$ is modeled as an ABX_3 halide perovskite, with potassium (K) at the A site, tin (Sn) at the B site, and iodine (I) at the anion site. The calculations reported in this work are restricted to the ideal cubic perovskite structure (space group $Pm\bar{3}m$, No. 221), characterised by a corner-sharing SnI_6 framework (Yadav and Sharma, 2024). No tetragonal or orthorhombic trial structures or phase comparisons are included in the present study. A variable-cell relaxation was performed for the cubic model, optimising the lattice parameter and internal coordinates subject to cubic symmetry.

Periodic density functional theory calculations were performed using Quantum ESPRESSO 7.2 and the generalised-gradient approximation of Perdew, Burke, and Ernzerhof (PBE) for structural optimisation. The computational protocol used scalar-relativistic pseudopotentials for geometry optimisation and fully relativistic datasets for electronic calculations. The kinetic-energy cutoff was 80 Ry, and the charge-density cutoff was 640 Ry. Brillouin-zone integrations used an 8 × 8 × 8 Monkhorst–Pack mesh. Marzari–Vanderbilt smearing of 0.01 Ry was applied during relaxation to aid Brillouin-zone integration; final properties were evaluated using an 8 × 8 × 8 mesh. Structural optimisation convergence criteria were a total-energy change below 10^{-8} Ry per atom, residual forces below 10^{-4} Ry $Bohr^{-1}$, and residual stress below 0.5 kbar.

The optimised cubic geometry and its total energy were used as the structural input for the electronic and optical calculations, without further geometric modification. This separation was adopted to avoid unintended structural changes between calculation stages (Yan et al., 2024). No van der Waals correction was applied because the

modeled structure is a three-dimensional ionic/covalent Sn-I network.

RESULTS AND DISCUSSION

Evidence Status and Structural Model

The section presents the results of an optimized cubic representation of $KSnI_3$, as illustrated in Figure 1a. In this structure, potassium (K) atoms are situated at the large peripheral sites, while tin (Sn) resides within an iodide octahedron. The iodide ions create an octahedral coordination environment, confirming the visualization of a cubic structural model (Yousfi et al., 2025). However, the analysis does not confirm that this structure represents the lowest-energy phase, nor does it assert that the unit cell is fully relaxed or that all residual forces and stresses meet the desired thresholds.

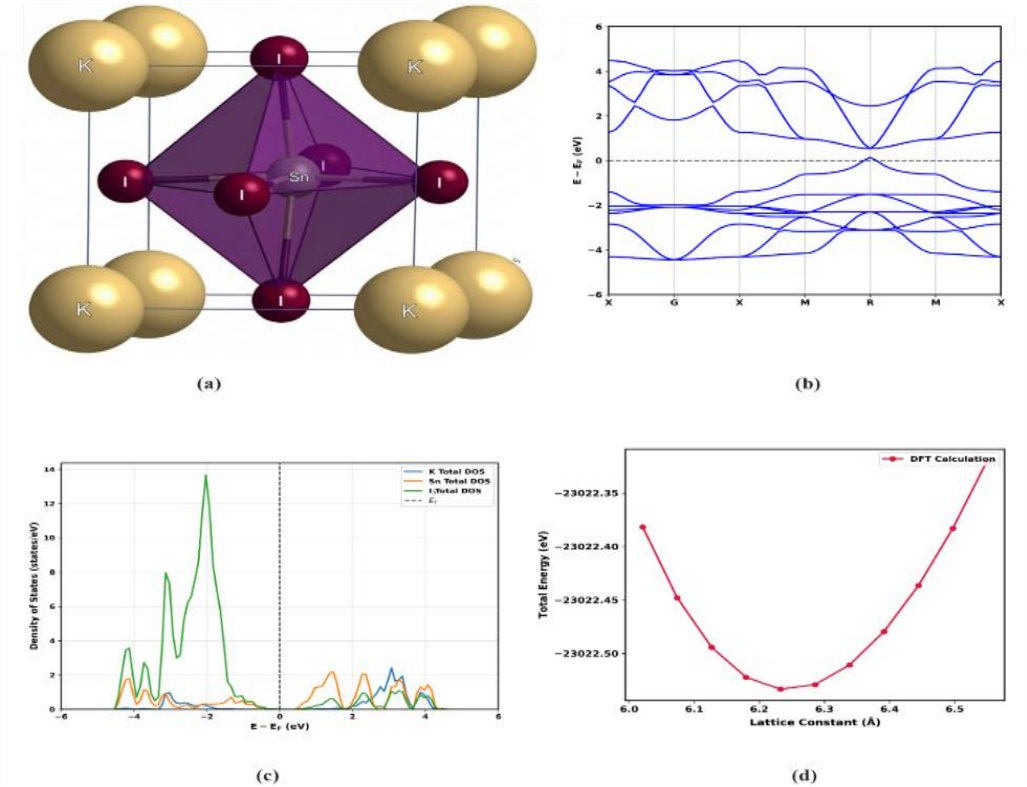


Figure 1: Electronic Structure and Optoelectronic Properties of $KSnI_3$ (a) optimised cubic crystal structure. (b) The electronic band structure. (c) Density of states (DOS). (d) Total energy as a function of the lattice constant (Yousfi et al., 2025)

Crystal Structure and Energetic Optimisation

The structural analysis of $KSnI_3$ in figure 1a, reveals an iodide perovskite framework where potassium (K) resides in the larger A-site cavity and tin (Sn) is octahedrally coordinated with iodide. The total-energy curve demonstrates a minimum near a lattice constant of approximately 6.3 Å, indicating an optimized equilibrium lattice scale for the structure. However, this observation alone cannot confirm global thermodynamic stability, as further assessments concerning formation energy against competing phases, elastic stability, phonon dispersion, and finite-temperature effects are essential (Verma et al., 2023). The orthorhombic arrangement is scientifically justifiable and aligns with prior density functional theory (DFT) findings on $KSnI_3$. The equilibrium lattice parameter of cubic $KSnI_3$ (a=b=c) was determined by fitting the calculated total-energy-lattice-parameter data using Quantum ESPRESSO's ev.x equation-of-state tool. The optimized lattice parameter was found to be approximately, $a_0 =$ 6.30Å. (Siddique et al., 2026).

Electronic Structure

The band plot in figure 2b, shows the electronic band structure of $KSnI_3$ was calculated using density functional theory (DFT) implemented in Quantum ESPRESSO 7.2. The calculated band gap equals 0.75 eV, indicating narrow-band-gap semiconducting behaviour and potential relevance to photovoltaic and optoelectronic applications. The density of states (DOS) plot shows strong features for occupied states below the Fermi level and unoccupied states above it. Notably, the dispersion of bands indicates varying degrees of dispersiveness, which impacts effective mass and transport properties (Mushtaq et al., 2025). However, the precise determination of the gap's

direct or indirect nature requires analysis of the band extrema and k-point coordinates, not just visual assessment. This electronic structure aligns with the significance of Sn-I orbital hybridization in tin iodide perovskites (Kavitha and Sudheer, 2026). It is important to note that the reported gap is method-dependent and doesn't confirm whether spin-orbit coupling (SOC) was included or the precise theoretical approach used, such as PBE or hybrid functionals. The 0.75 eV value should be considered as indicative rather than universally experimental, necessitating further investigations into scalar relativistic versus SOC calculations, functional dependence, and detailing effective mass tensors and orbital projections at both band edges.

Density of States (DOS)

The analysis of the Density of States (DOS) for $KSnI_3$, as shown in Figure 1c, highlights notable electronic contributions from atomic orbitals, with a clear dominance of I-5p states in the valence band (VB). A significant peak around -2 eV reflects a high density of iodine states vital for valence band formation (Sanni et al., 2026). Additionally, strong hybridization between Sn-5s and I-5p states near the valence band maximum (VBM) enhances both charge transfer and the covalent nature of the Sn-I bond (Saiful et al., 2023). In contrast, the conduction band (CB) is predominantly made up of Sn-5p states, which are crucial for electron transport; K states demonstrate minimal involvement, primarily serving structural roles. This suggests that K+ does not substantially affect the electronic properties near the band gap, reinforcing the conclusion that $KSnI_3$ is semiconducting in nature.

Lattice Optimisation

The total energy of cubic $KSnI_3$ was calculated as a function of the cubic lattice parameter, as shown in Fig. 1d. The resulting energy-lattice-parameter curve exhibits a minimum at approximately 6.30Å; this value is taken as the equilibrium lattice parameter of the cubic model within the present computational setup. The curve therefore provides the basis for identifying the optimised lattice parameter. It does not, by itself, establish thermodynamic stability, mechanical stability, or suitability for device operation. No direct comparison is made between this cubic lattice parameter and a lattice parameter reported for orthorhombic $KSnI_3$, because the structures have different symmetries. Establishing relative phase stability would require explicitly comparable calculations of the candidate structures under consistent computational settings and appropriate energetic criteria.

Optical Properties

The optical response of $KSnI_3$ demonstrates a structured energy-dependent behaviour from low energies up to about 20 eV, indicating its potential as an optically active semiconductor. The absorption coefficient remains low (nearly zero) up to approximately 2.3-2.5 eV, sharply increasing thereafter, with significant absorption peaks occurring between 2.7-4.2 eV, and strong absorption noted from 6 eV up to around 12.5 eV, peaking near 8.5-9.2 eV. A secondary absorption response between 18.5 to 20 eV is also observed. The dielectric function includes a real part that varies significantly near electronic transitions, and the imaginary component rises sharply correlating with absorption onset (Hasan et al., 2025). Additionally, the energy-loss function shows weak values below 3 eV, rising notably around 12.5 eV, indicative of collective electronic excitations.

Further, the extinction coefficient remains negligible at low energies, sharply increasing to a peak at around 3.1 eV and showing a broad response between 6 and 11 eV. Reflectivity increases until the absorption onset, with maximum values peaking between 11.5–12.7 eV, while the refractive index varies significantly, indicating strong polarizability and phase changes. Transmittance trends reveal oscillatory behaviour, with minimum values occurring at specific energy intervals, contributing to the assessment of solar energy applications (Rahman et al., 2026). Overall, $KSnI_3$'s complex optical characteristics underline its utility for thin-film applications, with a significant emphasis on factors beyond the optical response, such as carrier mobility and defect recombination, for effective photovoltaic performance.

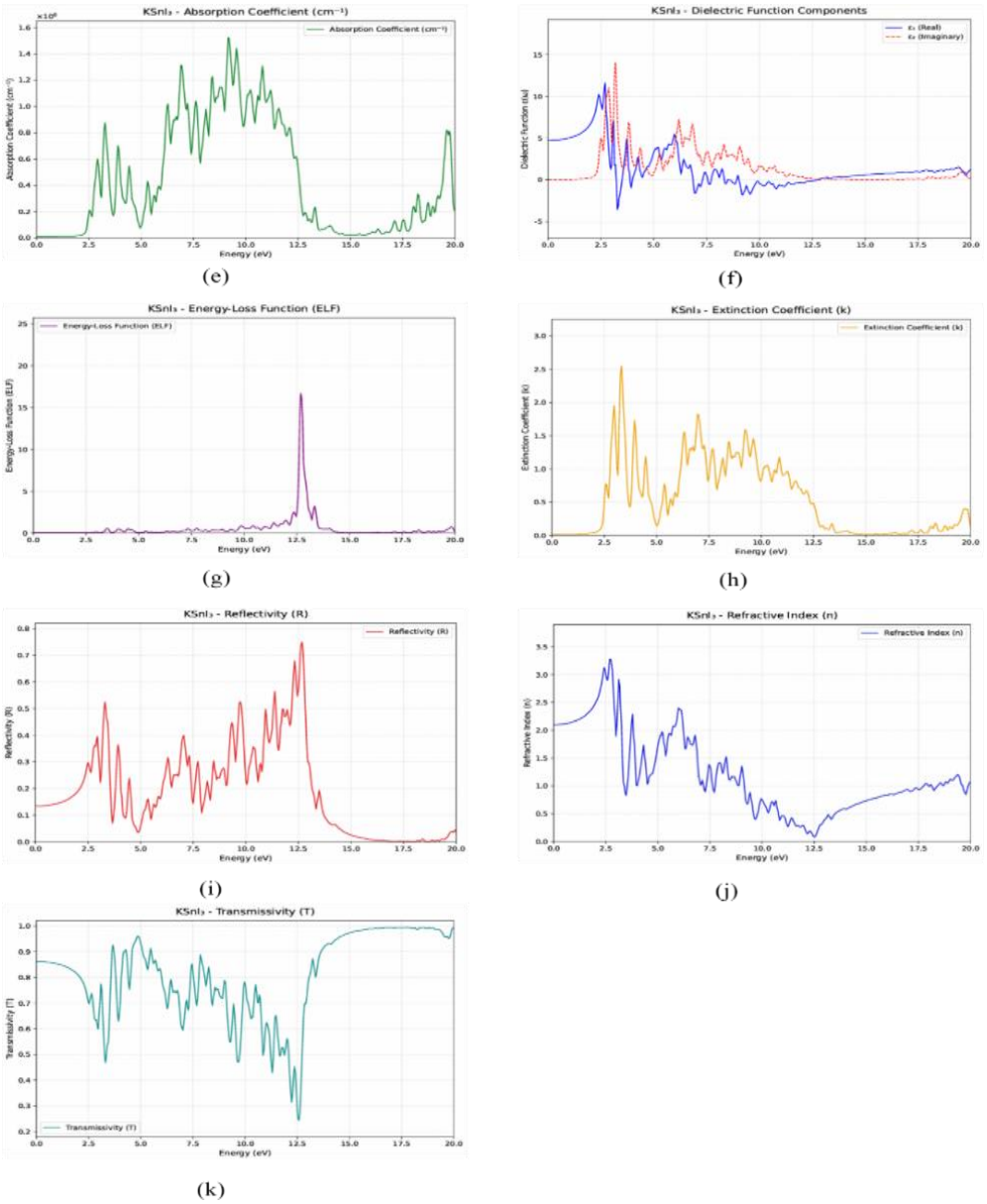


Figure 2: Optical Properties of $KSnI_3$ (a) Absorption Coefficient (cm^{-1}). (f) Dielectric Function Components (g) Energy-Loss Function (ELF). (h) Extinction Coefficient (k). (i): $KSnI_3$ Reflectivity (r). (j) Refractive Index (n). (k) Transmittance (T) (Hasan et al., 2025)

Conclusion

In this study, density functional theory (DFT) was employed to analyze the structural, energetic, electronic, and optical characteristics of $KSnI_3$, utilizing an orthorhombic perovskite model. The computational settings specified in the methods section led to an energy-lattice parameter curve with an optimization minimum around 6.3 Å, representing the optimized lattice scale. However, this value does not confirm the global stability of the $KSnI_3$ phase or match the experimentally established equilibrium structure. The electronic structure calculations revealed a finite band gap of about 0.75 eV, with iodine-derived states significantly contributing to the valence band and tin-derived states predominantly near the conduction band. These findings suggest that the model behaves like a semiconductor under the theoretical framework used, although the band-gap's nature and its dependence on various factors necessitate validation through further detailed calculations. The study also derived various optical properties, including the dielectric function, absorption coefficient, and transmittance, indicating the need for additional investigations into the optical response of $KSnI_3$. However, these properties should not be taken as indicators of photovoltaic performance. Importantly, the computations do not assess stability against Sn^{2+} oxidation, thermodynamic stability

vis-à-vis competing phases, or aspects such as defect tolerance and power-conversion efficiency. The implications of this research highlight the need for continued exploration of $KSnI_3$ as a potential photovoltaic absorber. Future investigations should include comparisons among different structural candidates-cubic, orthorhombic, tetragonal, and monoclinic-using consistent computational protocols, as well as assessments of formation energies, phonon dispersions, and elastic properties. Additionally, electronic and optical calculations should be repeated with careful documentation of spin-orbit coupling, oxidation chemistry, and related defect studies, supplemented by device-level simulations and experiments. These steps are crucial for differentiating theoretical predictions from practical material stability and photovoltaic capabilities.

REFERENCES

Aberle, A. G. (2009). Thin-film solar cells. *Thin Solid Films, 517(17), 4706–4710.* https://doi.org/10.1016/j.tsf.2009.03.056

Adebayo, S., Bamidele, A. A., Awodele, M. K., and Awodugba, A. O. (2026). $CsSn_xGe_{1-x}I_3$ lead-free perovskites: First-principles DFT analysis, stability, and optoelectronic properties. *10(1), 8–14.* https://doi.org/10.26480/aem.01.2026.08.14.

Adedokun, O., Sivaprakash, P., Ajani, A. S., Bello, I. T., and Arumugam, S. (2023). Structural, optical and magnetic studies of sol-gel synthesized Mg-doped pure anatase TiO_2 nanoparticles for spintronic and optoelectronics applications. *Physica B: Condensed Matter, 667, 415199.* https://doi.org/10.1016/j.physb.2023.415199

Ayvalik, A., Dogan, K. C., Cetin, Z., Yagmurcukardes, M., and Orucu, H. (2026). Strain-tunable electronic and optical properties of $KSnI_3$ perovskite polymorphs: From structural stability to optoelectronic potential. *ACS Omega, 11(18), 27128–27142.* https://doi.org/10.1021/acsomega.6c00784

Chatzisideris, M. D., Espinosa, N., Laurent, A., and Krebs, F. C. (2016). Ecodesign perspectives of thin-film photovoltaic technologies: A review of life cycle assessment studies. *Solar Energy Materials and Solar Cells, 156, 2–10.* https://doi.org/10.1016/j.solmat.2016.05.048

Chopra, K. L., Paulson, P. D., and Dutta, V. (2004). Thin-film solar cells: An overview. *Materials Science and Applications, 12(2–3), 69–92.*

Das, T., Di Liberto, G., and Pacchioni, G. (2022). Density functional theory estimate of halide perovskite band gap: When spin–orbit coupling helps. *The Journal of Physical Chemistry C, 126(4), 2184–2198.* https://doi.org/10.1021/acs.jpcc.1c09594

Deepika, K., Singh, A., and Ameen, S. (2025). Identifying recombination mechanisms in Sn-based perovskite/electron-transport-layer interface in perovskite devices using SCAPS-1D. *Physica Status Solidi (a), 222(10), 2400903.* https://doi.org/10.1002/pssa.202400903

Hasan, N., Khan, M. H., Mohammed, A., Hasan, M., Islam, S., & Kabir, A. (2025). Comprehensive numerical analysis of doping controlled efficiency in lead - free CsSn 1 − x Ge x I 3 perovskite solar cell. *Applied Physics A*, (2024). https://doi.org/10.1007/s00339-024-08125-y

Kavitha, M. V., & Sudheer, K. S. (2026). a numerical simulation study investigating the functionality of a perovskite solar cell based on fasni3 in both conventional and inverted configurations using compatible zn(o0.3s0.7) as the electron transport LAYER. *East European Journal of Physics*, *2026*(2), 292–301. https://doi.org/10.26565/2312-4334-2026-2-31

Kheswa, B. V., Majola, S. N. T., Al-Dmour, H., Ndzane, N. M., and Makhathini, L. (2025). Modeling and analysis of $KSnI_3$ perovskite solar cells yielding power conversion efficiency of 30.21%. *Nanomaterials, 15(8), 580.* https://doi.org/10.3390/nano15080580

Kundara, R., and Baghel, S. (2025a). Performance optimization of $CsSnI_3$-based perovskite solar cells using SCAPS-1D and machine learning analysis. *Journal of Optics, 55(4), 3494–3507.* https://doi.org/10.1007/s12596-025-02510-3

Kundara, R., and Baghel, S. (2025b). Performance optimization of lead-free $KGeCl_3$-based perovskite solar cells using SCAPS-1D. *Solar Energy, 287, 113253.* https://doi.org/10.1016/j.solener.2025.113253

Macdonald, T. J., Lanzetta, L., Liang, X., Ding, D., and Haque, S. A. (2023). Engineering stable lead-free tin halide perovskite solar cells: Lessons from materials chemistry. *Advanced Materials, 35(25), Article 2206684.* https://doi.org/10.1002/adma.202206684

Mushtaq, M., Jalil, A., Khan, R. A. S., Aamir, M., & Raza, S. R. A. (2025). Lead-Free KSnX3 [X = Cl, Br, F] Based Perovskite Solar Cell: A DFT Study and SCAPS Simulation. *Journal of Electronic Materials*, *54*(8), 6616–6629. https://doi.org/10.1007/s11664-025-12073-5

Pindolia, G., and Shinde, S. M. (2023a). Effect of organic charge transport layers on unleaded $KSnI_3$-based

perovskite solar cell. *Results in Optics, 12, 100469.* https://doi.org/10.1016/j.rio.2023.100469

Pindolia, G., and Shinde, S. M. (2023b). Effect of phthalocyanine-based charge transport layers on unleaded $KSnI_3$ perovskite solar cell. *Physica Scripta, 98(6), 065520.* https://doi.org/10.1088/1402-4896/acd4ff

Pindolia, G., and Shinde, S. M. (2023c). Unleaded all-inorganic $KSnI_3$ perovskite solar cell: A computational study. *Optik, 295, 171470.* https://doi.org/10.1016/j.ijleo.2023.171470

Rahman, F., Rahman, A., Sabrin, M. M., & Hossain, F. (2026). *Multiscale quantum-to-device simulation framework for Ca 3 AsBr 3 perovskite solar cells : engineering efficient electron transport layers*. 1–28.

Sabino, F. P., Zhao, X. G., Dalpian, G. M., and Zunger, A. (2024). Impact of symmetry breaking and spin–orbit coupling on the band gap of halide perovskites. *Physical Review B, 110(3), Article 035160.* https://doi.org/10.1103/PhysRevB.110.035160

Said, K., and Elkhattabi, S. (2024). Structural, electronic, and optical study of lead-free perovskite $CH_3NH_3SnBr_3$ under compressive strain using DFT and DFT+U. *Materials Science in Semiconductor Processing, 174, 108242.* https://doi.org/10.1016/j.mssp.2024.108242

Sharma, P., Ranjan, P., and Chakraborty, T. (2024). DFT and TD-DFT studies of perovskite materials $LiAX_3$ (A = Ge, Sn; X = F, Cl, Br, I) in reference to their solar-cell applications. *Materials Today Sustainability, 26, 100791.* https://doi.org/10.1016/j.mtsust.2024.100791

Saiful, M., Azizman, A., Wazira, A., Suriyani, D., Halin, C., Ibrahim, N., Sepeai, S., Ahmad, N., & Nuzaihan, M. (2023). Progress in tin-germanium perovskite solar cells : A review. Synthetic Metals, 299(April), 117475. https://doi.org/10.1016/j.synthmet.2023.117475

Sanni, D. M., Ndanusa, H. H., & Abubakar, H. (2026). Numerical Optimization of ZnO Electron Transport Layer and Absorber Properties with Temperature Effects in Germanium-Based Perovskite Solar Cells Using SCAPS-1D Simulation. Fudma Journal of Sciences, 10(ANB-K), 196–203. https://doi.org/10.33003/fjs-2026-10(anb-k)-5402

Siddique, A. F., Sadat, A., & Rahman, S. (2026). High efficiency lead-free AlSb / KSnI 3 - ACIGS monolithic 2 T tandem solar cells with theoretical efficiency above 39 percent.

Sumona, F. B., Kashif, M., Danladi, E., Tighezza, A. M., Al-Mahmud, N., Toki, G. F. I., Pandey, R., and Hossain, M. K. (2023). Optimization of perovskite-$KSnI_3$ solar cell by using different hole and electron transport layers: A numerical SCAPS-1D simulation. *Energy & Fuels, 37(23), 19207–19219.* https://doi.org/10.1021/acs.energyfuels.3c02397

Sundaram, S., Shanks, K., and Upadhyaya, H. (2018). Thin film photovoltaics. *In A comprehensive guide to solar energy systems (pp. 361–370). Academic Press.* https://doi.org/10.1016/B978-0-12-811479-7.00018-X

Tarekuzzaman, M., Ishraq, M. H., Shahadath, N., Kabir, M. R., Rayhan, M. A., Ahmad, S., Qader, M. A., Rasheduzzaman, M., Arafat, Y., and Hasan, M. Z. (2025). DFT analysis of structural, electronic, optical, and thermodynamic properties of $LiXI_3$ (where X = Ca, Sr, Ba) halide perovskites for optoelectronics. *Scientific Reports, 15, Article 25304.* https://doi.org/10.1038/s41598-025-91458-2

Verma, S., Ali, H., and Singh, P. (2023). Solar-powered transportation systems: From buses to aircraft prototypes. *Renewable Energy, 210, 531–542.*

Vishnupriya, G., and Sathya, P. (2025). Computational study of a novel combination of dual-absorber structured perovskite solar cell with theoretical efficiency of [title incomplete in supplied source]. *Frontiers in Energy Research, [volume/pages not supplied].* https://doi.org/10.3389/fenrg.2025.1631201

Wang, J., Lu, H., Pan, X., Xu, J., Liu, H., Liu, X., Khanal, D. R., Toney, M. F., Beard, M. C., and Vardeny, Z. V. (2020). Spin-dependent photovoltaic and photogalvanic responses of optoelectronic devices based on chiral two-dimensional hybrid organic–inorganic perovskites. *ACS Nano, 15(1), 588–595.* https://doi.org/10.1021/acsnano.0c05980

Wang, K., Chen, L., and Zhou, M. (2021). Perovskite–silicon tandem architectures: Design and performance. *Energy & Environmental Science, 14, 3580–3598.*

Wang, X., Liu, Y., and Patel, R. (2024). Challenges and solutions in scalable deposition of Sn–Ge mixed halide perovskites. *Nano Energy, 120, 108019.*

Wu, D., Huo, B., Huang, Y., Zhao, X., Yang, J., Hu, K., Mao, X., He, P., Huang, Q., and Tang, X. (2022). Synthesis of stable lead-free $Cs_3Sb_2(Br_xI_{1-x})_9$ ($0 \le x \le 1$) perovskite nanoplatelets and their application in CO_2 photocatalytic reduction. *Small, 18(12), Article 202106001.* https://doi.org/10.1002/smll.202106001

Wu, T., Liu, X., He, X., Wang, Y., Meng, X., and Noda, T. (2020). Efficient and stable tin-based perovskite solar cells by introducing π-conjugated Lewis base. *[Journal title not supplied], 63(1), 107–115.*

Yadav, P., and Sharma, R. (2024). Advanced quantum and nanostructural approaches in solar cells. *Progress in Quantum Electronics, 86, 100455.*

Yan, W., Zhu, M., Xin, F., and Zhou, Z. (2024). Alder–Ene reaction-mediated suppression of tin(II) oxidation for efficient tin–lead perovskite solar cells. *Angewandte Chemie International Edition, 136(43), Article e202409072.* https://doi.org/10.1002/ange.202409072

Yousfi, A., Saidani, O., Benmakhlouf, A., Helaimia, T., Alsubaie, A. S., Al Ahmed, S. R., and Islam, M. R. (2025). Design and simulation of high-efficiency $KSnI_3$-based perovskite solar cells using DFT and SCAPS-1D. *Scientific Reports, 15, Article 37022.* https://doi.org/10.1038/s41598-025-19579-2